Optimization of the Anisotropic United Atoms Intermolecular Potential for n-Alkanes

ARTICLE *in* THE JOURNAL OF CHEMICAL PHYSICS · MARCH 2000

Impact Factor: 2.95 · DOI: 10.1063/1.481116

6 AUTHORS, INCLUDING:

Philippe Ungerer
Materials Design S.A.R.L., Montrouge, France
117 PUBLICATIONS **2,663** CITATIONS
SEE PROFILE

Jerome Delhommelle
University of North Dakota
91 PUBLICATIONS **1,632** CITATIONS
SEE PROFILE

Optimization of the anisotropic united atoms intermolecular potential for *n*-alkanes

Philippe Ungerer
Department of Physical Chemistry, UMR 8611 CNRS, Université de Paris Sud, bât. 490, 91405 Orsay Cedex, France and Institut Français du Pétrole, 1-4 Av. de Bois Préau, 92852 Rueil-Malmaison Cedex, France

Christèle Beauvais, Jérôme Delhommelle, Anne Boutin, Bernard Rousseau, and Alain H. Fuchs
Department of Physical Chemistry, UMR 8611 CNRS, Université de Paris Sud, bâtiment 490, 91405 Orsay Cedex, France

(Received 6 August 1999; accepted 20 December 1999)

The parameters of the anisotropic united atoms potential for linear alkanes proposed by Toxvaerd [S. Toxvaerd, J. Chem. Phys. **107**, 5197 (1997)] have been optimized on the basis of selected equilibrium properties (vapor pressures, vaporization enthalpies, and liquid densities) of ethane, *n*-pentane, and *n*-dodecane. The optimized parameters for the CH_2 and CH_3 groups form a regular sequence with those of methane and the force centers are found between the carbon and hydrogen atoms, as expected. The resulting potential, called AUA4, has been compared with Toxvaerd's potential (AUA3) by using several molecular simulation methods (Gibbs ensemble Monte Carlo, thermodynamic integration, and molecular dynamics). An investigation performed at temperatures ranging from 140 to 700 K and with various chain lengths up to 20 carbon atoms has shown AUA4 to provide systematic improvements of vapor pressures, vaporization enthalpies, and liquid densities for pure *n*-alkanes. Significant improvements have been also noticed on the critical temperatures of *n*-alkanes, estimated from coexistence density curves, and on the equilibrium properties of CO_2–*n*-alkane binary mixtures. Self-diffusion coefficients of *n*-hexane, however, are slightly improved by the new potential, but still exceed experimental measurements at low temperature. As we have only optimized the intermolecular potential in the present study, it is suggested that further optimization of the intramolecular potentials of the anisotropic united atoms model could allow simultaneous prediction of thermodynamic properties and of transport coefficients, particularly in very dense liquids. © *2000 American Institute of Physics*. [S0021-9606(00)50211-6]

I. INTRODUCTION

In order to model fluid properties for industrial applications, molecular simulation presents the advantage of providing a unified theoretical framework for the prediction of equilibrium and transport properties. However, exploiting this advantage requires that transferable potential models are available to describe the inter- and intramolecular energy. Compared with potentials where all atoms are considered, those introducing groups like CH_2 or CH_3 as Lennard-Jones interaction sites allow to consider larger systems and/or longer simulations, which is very useful for applications. In this respect, several authors have developed united atoms potentials (UA) to represent equilibrium properties of *n*-alkanes[1–4] and isoalkanes[5] with a good accuracy. It seems likely that only marginal improvements of the UA potential can be expected after this abundant work.

While each force center is located on the carbon atom in the UA potentials, it has been proposed[6,7] to shift the force center so that it is placed between the carbon and hydrogen atoms of the related group. The resulting potential, called anisotropic united atoms (AUA) has been claimed to account simultaneously for equilibrium and transport properties.[7,8] However, it has been recently observed[9] that the prediction of the coexistence curve of *n*-dodecane was not very satisfactory with the last version of Toxvaerd's potential[7] that we will term here AUA3. Also, the AUA3 potential has been shown to underestimate the viscosity of dense liquids.[10,11] The authors of the AUA3 potential have imposed equal Lennard-Jones diameters for the CH_2 and CH_3 groups, while the latter is expected to be somewhat larger. Also, a ratio of 1.5 was imposed between the energetic parameters of the CH_2 and CH_3 groups on the basis of semitheoretical grounds. Both constraints can be released without compromising the general validity of the method, and it may be hoped that substantial improvements of the AUA potential will result. Another feature that could be improved in the potential is the selection of the bond lengths and average bond angles. Indeed, the authors of the AUA3 potential have used experimentally-derived values which vary slightly with carbon number, so that the potential cannot be readily applied to long chain alkanes for which no experimental values are available.

In the present work, it is therefore proposed to perform a simultaneous optimization of the Lennard-Jones interaction parameters of the CH_2 and CH_3 groups, including the offset distances separating the interaction site from the related carbon atom. For this, we select unique values for the carbon–

carbon distances and for average bond angles. Indeed, these parameters have a small influence in their possible range of variation.[9] However, we keep the intramolecular potential proposed by Toxvaerd[7] on the basis of recent spectroscopic data. In order to maximize the generality of the optimized potential, we use a set of reference experimental data covering a broad range of carbon numbers (ethane to *n*-dodecane) and temperatures (140 to 550 K) in the course of optimization. For the same reason, we fit simultaneously various equilibrium properties (vapor pressures, liquid densities, and vaporization enthalpies). This is also a way to maximize the use of every simulation run in the optimization process. However, we do not try to fit the critical properties explicitly, because the Gibbs ensemble Monte Carlo method used to compute phase equilibria would require an excessive amount of computer time.

Once the parameters are optimized, the new AUA potential and AUA3 are compared with measured equilibrium properties. This comparison is particularly aimed at testing the predictive capability of the potential on alkanes that are not part of the reference set. We extend this comparison to vapor pressures at low temperatures, in order to check that the chemical potential is well represented in the liquid phase. Also, the potential is applied to the coexisting density curves at higher temperatures (so that critical properties can be derived) and to binary mixtures of *n*-alkanes and carbon dioxide. Finally, we examine whether or not transport properties are well reproduced in dense liquid alkanes and conclude on the transferability of the new potential.

II. SIMULATION METHODS

A. Gibbs Ensemble Monte Carlo

In order to compute phase equilibria, we have used the Gibbs ensemble Monte Carlo method introduced by Panagiotopoulos,[12] associated with the configurational statistical bias method of Smit *et al.*[13] We have also included an additional bias for the insertion of the first center of the chain.[14] Details about the algorithms used can be found elsewhere.[15] The selected occurrences for the various types of moves were generally 0.1 for translations, rotations, and regrowth, 0.695 for transfers, and 0.005 for volume changes. Most simulations were made using a total number of 200 molecules. A cutoff radius of 10 Å was used, using standard long range corrections.[16]

After stabilization, vapor pressure was taken as the average pressure in the vapor simulation box over 1.5 to 4 $\times 10^6$ elementary steps. The precision on vapor pressure has been found to be 5%–10% in the favorable range of reduced temperatures for the Gibbs ensemble method, i.e., for $0.6 < T/T_c < 0.95$. In the lower part of this temperature range ($0.6 < T/T_c < 0.8$), the low rate of transfer between the vapor and the liquid causes the uncertainty to grow because pressure fluctuations are slow in the vapor phase. In order to accelerate this process, the global volume was selected in such a way that the average number of molecules in the vapor phase was low (typically 5 to 30). In the upper part of the temperature range ($0.85 < T/T_c < 0.95$), larger box sizes and finite size scaling would be needed to maintain a good accuracy. This is why high temperature phase equilibria have not been used in the course of optimization, but only in the process of evaluating the optimized potential.

The molar vaporization enthalpy is simply computed as the difference between the average molar enthalpies of the liquid and of the vapor simulation boxes. The statistical uncertainty on this property is typically 1% to 2%. We have noticed that the molar intramolecular energy was identical in coexisting phases within the statistical error. As we will see in the next section, this observation is useful for thermodynamic integration. It may be explained by the equipartition energy principle, which states that the average potential energy is $kT/2$ per harmonic oscillator.

The average liquid density was generally determined with a statistical uncertainty of 0.5% to 1%, but higher values (up to 5%) were found at near-critical temperatures. When vapor–liquid coexistence density curves were computed, the critical temperature was obtained by fitting the critical scaling law $\rho_l - \rho_g = \lambda (T_c - T)^{0.325}$. The law of rectilinear diameters was then used to estimate the critical density. These simulations have been performed with a total number of 200 molecules, except those related to *n*-pentane with the AUA3 potential where 400 molecules were introduced.

B. Thermodynamic integration

As mentioned above, the Gibbs ensemble method is poorly efficient for reduced temperatures (T/T_c) lower than 0.6. In order to extend the computation of vapor pressures to lower temperatures, we have integrated the Clapeyron equation as proposed by Kofke[17] with some modifications. At first, we use the identity of intramolecular energies in coexisting phases to estimate the molar vaporization enthalpy from a single monophasic simulation at constant pressure:

$$\Delta H_{\mathrm{vap}} \approx -E_l^{\mathrm{inter}} + RT, \tag{1}$$

where E_l^{inter} is the average molar intermolecular potential energy of the liquid simulation box. This relationship is obtained by neglecting the molar volume of the liquid vs. the vapor and assuming the vapor to be an ideal gas with zero intermolecular energy. These assumptions are indeed justified for reduced temperatures lower than 0.6, which correspond to vapor pressures significantly lower than atmospheric pressure. As will be shown later, the simplified way of estimating the vaporization enthalpy through Eq. (1) has been found consistent with the more rigorous application of the Gibbs ensemble method at higher temperatures.

The Clapeyron equation was integrated under the following form:

$$\left(\frac{d \ln P_{\mathrm{sat}}}{d(1/T)}\right) = -\frac{\Delta H_{\mathrm{vap}}}{R}. \tag{2}$$

An integration scheme of second order has been used with regularly spaced $1/T$ values:

$$\ln P_{\mathrm{sat}}^{(n+1)} = \ln P_{\mathrm{sat}}^{(n-1)} - \frac{\Delta H_{\mathrm{vap}}^{(n)}}{R}\left(\frac{1}{T^{(n+1)}} - \frac{1}{T^{(n-1)}}\right). \tag{3}$$

TABLE I. Compilation of saturated carbon–carbon bond distances and C–C–C bond angles in hydrocarbons.

Hydrocarbon	C–C distance (Å)	C–C–C bond angle (deg)
Ethane[a]	1.535	Ø
Propane[a]	1.532	112
n-butane[a]	1.531	113.8
n-pentane[b]	1.527 to 1.544	112.8 to 116.3
n-hexane[b]	1.527 to 1.544	112.2 to 117.7
Isobutane[a]	1.535	110.8
Cyclopentane[a]	1.546	Ø
Cyclohexane[a]	1.536	111.3
Cyclodecane[c]	1.545	114.6 to 116.9
Toluene ($C–CH_3$ bond)[a]	1.524	Ø

[a]Reference 19.
[b]Reference 21.
[c]Reference 20.

TABLE II. AUA4 potential parameters for molecular weight, carbon to carbon distance, bending potential, and torsion potential.

Molecular weight (g/mol)	CH_2	14.03
	CH_3	15.03
C–C distance (Å)		1.535
Bending[a]	θ_0 (deg)	114
	k_{bend} (K)	62500
Torsion[a]	a_0 (K)	1001.35
	a_1 (K)	2129.52
	a_2 (K)	−303.06
	a_3 (K)	−3612.27
	a_4 (K)	2226.71
	a_5 (K)	1965.93
	a_6 (K)	−4489.34
	a_7 (K)	−1736.22
	a_8 (K)	2817.37

[a]Reference 7.

The selection of a second-order scheme rather than higher-order algorithms is justified by the accuracy of the vaporization enthalpy. Using a scheme of order p requires that the computation of the derivative, i.e., the vaporization enthalpy, is accurate to the order $(p-1)$. As we will see in the application of the method, this is indeed the case. Incidentally, the second-order integration scheme has a favorable behavior with respect to the propagation of errors. It may be shown indeed that if the determination of ΔH_{vap} is unbiased, most of the statistical errors on ΔH_{vap} of successive points cancel out in the course of integration. As the relative uncertainty is low on vaporization enthalpies, the relative uncertainty on extrapolated vapor pressures is mainly limited by the Gibbs ensemble results used as starting points.

C. Molecular dynamics

The molecular dynamics calculations have been performed by using the RATTLE algorithm to solve the constrained equations of motion, as developed in previous work for the transport properties of flexible molecules.[10,18] The simulations of *n*-hexane have been performed in the canonical ensemble with 108 molecules, using a Nose–Hoover thermostat.[10] The self-diffusion coefficient has been computed through an analysis of the mean-square displacement r vs time:

$$D=\frac{1}{6}\frac{d\langle (r(0)-r(t))^2\rangle}{dt}. \tag{4}$$

III. PARAMETER DETERMINATION

A. Carbon–carbon distances and average bond angles

A brief compilation of average lengths for saturated carbon–carbon bonds in various hydrocarbons (Table I) indicates that their values are comprised between 1.524 and 1.545 Å. As a consequence of the small amplitude of these variations, we have decided to set the carbon–carbon distance to 1.535 Å. This value is very close from the 1.534 Å selected by Fitzwater and Bartell[22] and to the 1.53 or 1.54 Å selected by the authors of various united atoms potentials.[2–4]

Similarly, the average C–C–C bond angles of saturated hydrocarbons (Table I) show values between 110.8 and 116.9 deg. We have therefore selected a unique value $\theta_0 = 114$ deg, identical to the average angle of the TRAPPE and NERD potentials,[3,4] slightly greater than in the SKS potential.[2] The expressions for the torsion potential $U^{tors}/k = \Sigma_{j=0}^{8} a_j(\cos\phi)^j$ and for the bending potential $U^{bend}/k = \frac{1}{2}k_{bend}(\cos\theta-\cos\theta_0)^2$ have been taken identical to those of Toxvaerd[7] with the same parameters a_j and k_{bend} (Table II), k being the Boltzmann constant.

B. Reference data

The selection of the reference components has been made in order to identify precisely the contributions of the CH_2 and CH_3 groups to *n*-alkane properties. These components include *n*-pentane and *n*-dodecane, where CH_2 is the major group, and ethane where CH_3 only is represented. For each component, we introduced vapor pressures, vaporization enthalpies, and liquid densities as reference data.

The reason for selecting vapor pressures rather than vapor densities is that more direct measurements are available, so that the experimental information is more reliable. However the GEMC algorithm requires long computing times at low temperatures (because of the low acceptance rate of transfer moves) and at near-critical temperatures (because of fluctuations, which require use of large simulation boxes if a good accuracy is desired). Therefore we decided to select a unique reference vapor pressure for each compound, at a reduced temperature (T/T_c) of approximately 0.8 where GEMC is efficient. Thanks to the introduction of the vaporization enthalpy and liquid density as reference data, a good extrapolation capability toward lower and higher temperatures is expected because these properties control the temperature dependence of the vapor pressure through the Clapeyron equation. In order to extend the applicability of the potential to low temperatures, we have also introduced liquid density and vaporization enthalpy at a low reduced temperature $(T/T_c = 0.5$ or less) for each component. As the equilibrium pressure is very low at such temperatures, these properties were computed from a monophasic simulation of the liquid phase in the NPT ensemble at $P=0$, using Eq. (1) for

the vaporization enthalpy. Per component, two simulations (one GEMC run and one monophasic NPT run) allow us to compare a given potential with five independent experimental data. Compared with the usual approach of fitting the coexisting density curve with GEMC simulation results, our procedure maximizes the exploitation of simulation runs and addresses a larger temperature range.

The reference data and their sources are indicated by Table II. As far as possible, we used raw data, such as those published in the compilation of Vargaftik.[23] In several cases, we used the correlations provided by the Dortmund Data Bank[24] instead of raw data, after having checked their validity on available measurements at other temperatures. These were particularly useful for vapor pressures, since these correlations provide a well-established average between numerous selected data sources of the literature.

C. Optimization method

In order to fit simultaneously various properties with different dimensions, we have used the following dimensionless error criterion:

$$F=\frac{1}{n}\sum_{i=1}^{n}\frac{(X_i^{\mathrm{mod}}-X_i^{\mathrm{exp}})^2}{s_i^2}, \tag{5}$$

where s_i is the estimated statistical uncertainty on the computed variable X_i^{mod}, while X_i^{exp} is the associated experimental measurement [either $\ln(P_{\mathrm{sat}})$, ΔH_{vap}, or ρ_e]. F is considered as a function of the six parameters to optimize, namely the interaction energies $y_1=\epsilon(\mathrm{CH_3})$ and $y_2=\epsilon(\mathrm{CH_3})$, the molecular diameters $y_3=\sigma(\mathrm{CH_2})$ and $y_4=\sigma(\mathrm{CH_3})$, and the carbon-to-center distances $y_5=\delta(\mathrm{CH_2})$ and $y_6=\delta(\mathrm{CH_3})$. The minimum condition for F is that every partial derivative $\partial F/\partial y_j$ must be zero:

$$\frac{\partial F}{\partial y_j}=\frac{1}{n}\sum_{i=1}^{n}\frac{2(X_i^{\mathrm{mod}}-X_i^{\mathrm{exp}})\dfrac{\partial X_i^{\mathrm{mod}}}{\partial y_j}}{s_i^2}=0 \quad \text{for } j=1,...,6. \tag{6}$$

This expression was estimated through a first-order Taylor expansion of X_i^{mod} around the point y^o corresponding to the AUA3 potential:

$$X_i^{\mathrm{mod}}(y^o+\Delta y)=X_i^{\mathrm{mod}}(y^o)+\sum_{k=1}^{6}\frac{\partial X_i^{\mathrm{mod}}(y^o)}{\partial y_k}\Delta y_k$$

$$\text{for } i=1,...,n.$$

The minimum condition, Eq. (6) can then be expressed as:

$$\sum_{i=1}^{n}\frac{\left[X_i^{\mathrm{mod}}(y^o)-X_i^{\mathrm{exp}}+\Sigma_{k=1}^{6}\dfrac{\partial X_i^{\mathrm{mod}}}{\partial y_k}\Delta y_k\right]\dfrac{\partial X_i^{\mathrm{mod}}}{\partial y_j}}{s_i^2}=0. \tag{7}$$

In this expression the derivatives $\partial X_i^{\mathrm{mod}}/\partial y_k$ have been evaluated by finite differences at the point y^o. Once these derivatives are known, the Δy_k may be obtained by solving a linear system of six equations and six unknowns, yielding the optimized parameters through $y_k=y_k^o+\Delta y_k$.

D. Optimization results

The evaluation of the deviation F and its partial derivatives required 36 simulations. The total computing time required for this optimization has been 1200 h of single processor on a SGI Origin2000 computer, which is still reasonable. Among other features, the determination of partial derivatives has shown that the three properties investigated (vapor pressures, vaporization enthalpies, and liquid densities) were highly influenced by the offset distance of the CH_2 and CH_3 groups.

The results of the optimized potential (AUA4) are compared with Toxvaerd's potential[7] (AUA3) on the basis of the reference data points in Table III. The average dimensionless error, i.e., the square-root of expression (5), is greatly improved, since it changes from $F^{1/2}=4.2$ in the AUA3 potential to $F^{1/2}=0.53$ in AUA4. This is mainly due to the improvement of the liquid densities of ethane and of the equilibrium properties of *n*-dodecane (vapor pressure, vaporization enthalpy). A small improvement is obtained on *n*-pentane properties, which are already well represented by AUA3. It may be noticed that most reference data are reproduced within the estimated statistical uncertainty.

The optimized parameters, as indicated by Table IV, are not dramatically changed. Compared with AUA3, the CH_2 group has a smaller diameter while CH_3 is larger. The energetic parameter of the CH_2 group is significantly increased.

IV. EVALUATION OF THE OPTIMIZED POTENTIAL

A. Equilibrium properties of *n*-alkanes

In order to test its applicability, the optimized AUA4 potential has been tested against various data that were not included in the reference data set. In the case of *n*-pentane and *n*-eicosane, GEMC simulations and monophasic NPT simulations have been performed in a large temperature range, extending far below the normal boiling point, in order to compare the potential with vapor pressures through thermodynamic integration (Table V, Fig. 1). A few simulations have also been performed for propane and *n*-octane, particularly at the normal boiling temperature. As illustrated by Figs. 1, 2, 3, the AUA4 potential predicts very well the properties of *n*-alkanes in the investigated conditions.

In order to test the ability of the potential to reproduce the critical parameters, a determination of the coexisting density curves of *n*-pentane, *n*-decane, and *n*-dodecane has been performed (Table VI, Figs. 4, 5, 6). This yielded critical temperatures in better agreement with experimental data than the AUA3 potential (Table VII).

Additional simulations have been performed with the TRAPPE united atoms potential, using the latest parameter set of Martin and Siepmann[5] ($k=46$ K and $\sigma=3.95$ Å for CH_2, $\epsilon/k=98$ K and $\sigma=3.75$ Å for CH_3) which was slightly modified compared with the original set[3] published by the same authors. The results (Table VIII) show a very satisfactory representation of liquid densities (Fig. 3), but also a systematic underestimation of vaporization enthalpies over the whole temperature range investigated (Fig. 2), while vapor pressures appear overestimated at low temperatures (Fig. 1).

TABLE III. Summarized table of the optimization of the AUA potential with all reference data points. AUA3 stands for the potential published by Toxvaerd (Ref. 7) and AUA4 stands for the optimized AUA parameters. Vapor pressures (P_{sat}) are expressed in kPa, vaporization enthalpies (ΔH_{vap}) in kJ/mol, and liquid densities (ρ_l) in kg/m^3.

Reference compound	T(K)	Simulation conditions	Type of data	Experimental data	Estimated statistical uncertainty	AUA3	AUA4
Ethane	240	GEMC	P_{sat}	966[a]	100	968	945
			ΔH_{vap}	12.0[a]	0.5	12.31	11.97
			ρ_l	472[a]	10	513	471
	140	monophasic	ΔH_{vap}	16.36[a]	0.5	15.97	15.91
		NPT, $P=0$	ρ_l	598[a]	5	652	600
*n*C5	385.82	GEMC	P_{sat}	775[a]	100	866	765
			ΔH_{vap}	20.25[a]	0.5	19.14	20.36
			ρ_l	521[b]	10	512	521
	232.3	monophasic	ΔH_{vap}	29.6[b]	0.5	28.4	29.55
		NPT, $P=0$	ρ_l	683[b]	5	697	689
*n*C12	550	GEMC	P_{sat}	355[b]	100	600	350
			ΔH_{vap}	37.45[a]	1	30.73	37.57
			ρ_l	530[a]	10	486	531
	305.57	monophasic	ΔH_{vap}	60.15[a]	1	55.10	59.37
		NPT, $P=0$	ρ_l	740[b]	5	723	746

[a]Correlations of the Dortmund data bank (Ref. 24), version 1998.
[b]Interpolated from Vargaftik (Ref. 23).

B. Phase equilibria of binary mixtures of *n*-alkanes and carbon dioxide

The P,x phase diagrams of CO_2–*n*-pentane and CO_2–*n*-decane mixtures have been computed at 344.16 and 477 K, respectively, using the potential of Harris and Yung[27] for carbon dioxide (Table IX, Figs. 7 and 8). In both cases, a significant improvement is observed compared with previous simulations of the same mixtures with the AUA3 potential.[30]

For the CO_2–*n*-pentane system, the phase densities were found in good agreement with the experimental measurements of Besserer and Robinson.[28] For the CO_2–*n*-decane mixture (Fig. 9) the AUA4 potential provides a better prediction of the liquid density than the AUA3 potential by comparison with the data of Reamer and Sage.[29]

C. Self-diffusion coefficients of liquid *n*-hexane

A preliminary series of molecular dynamics simulations has been performed to compare the self-diffusion coefficients predicted with the AUA4 and AUA3 potentials with the experimental measurements of Harris.[31] The comparison has been made for temperatures ranging from 223 to 333 K at atmospheric pressure. For this purpose, the simulations have been performed at the experimental density indicated by Harris.[31] The results (Table X, Fig. 10) show that the decreasing trend of self-diffusion coefficients is well reproduced, but a significant underestimation is noticed in the lower part of the temperature range. A slight improvement is noticed compared with AUA3. It has been observed during these simulations that the pressure was negative, indicating that the density of liquid *n*-hexane was underestimated by the AUA4 potential at very low temperature.

TABLE IV. Comparison of the optimized AUA parameters (AUA4) with those of Toxvaerd[a] (AUA3).

	CH_2		CH_3	
	AUA3	AUA4	AUA3	AUA4
ϵ/k (K)	79.87	86.291	119.8	120.15
σ (Å)	3.516	3.4612	3.516	3.6072
δ (Å)	0.40	0.38405	0.18	0.21584

[a]Reference 7.

V. DISCUSSION

The optimized molecular diameters of CH_2 (3.4612 Å) and CH_3 (3.6072 Å) indicated in Table III form a regular sequence with methane[32] (3.7327 Å). Similarly the optimized interaction energies of CH_2 (86.291 K), CH_3 (120.15 K) and methane[32] (149.92 K) are regularly spaced. The offsets ($\delta=0.384\,05$ Å for CH_2 and $\delta=0.215\,84$ Å for CH_3) place the group centers close to the estimated geometrical centers of the CH_2 group ($\delta_g=0.42$ Å) and CH_3 ($\delta_g=0.27$ Å). These observations clearly show that the optimization has converged toward values that have a good physical meaning. In order to illustrate the position of the force center and the exclusion sphere (diameter σ) of both groups, we have compared them with the exclusion spheres of their constituting atoms, using the Lennard-Jones parameters of the OPLS potential,[33] i.e., $\sigma=3.5$ Å for carbon and $\sigma=2.5$ Å for hydrogen. In the case of CH_2 (Fig. 11), the exclusion sphere of the group is not larger than the carbon exclusion sphere, but it is shifted so that there is more overlap with the two hydrogens. In the case of the CH_3 group (Fig. 12), the exclusion sphere is somewhat larger than the carbon sphere, as needed to increase the overlap with the three hydrogens, and the shift is less important.

TABLE V. Application of the optimized AUA potential (AUA4) and of the AUA potential of Toxvaerd (Ref. 7) (AUA3) in conditions outside the reference data set, at low reduced temperatures. Vapor pressures (P_{sat}) are expressed in kPa, vaporization enthalpies (ΔH_{vap}) in kJ/mol, and liquid densities (ρ_l) in kg/m^3.

Compound	T (K)	Simulation method	Property	Experimental data	AUA3	AUA4
Propane	231.1	GEMC	P_{sat}	100[a]		83.9
			ΔH_{vap}	19.04[b]		18.41
			ρ_l	582[a]		582
n-pentane	356.38	GEMC	P_{sat}	399[b]	454	375
			ΔH_{vap}	22.6[b]	21.5	23.1
			ρ_l	559[c]	554	564
	331.11	GEMC	P_{sat}	208[b]	217	192
			ΔH_{vap}	24.4[b]	23.2	24.4
			ρ_l	587[c]	584	590
	309.2	GEMC	P_{sat}	100[b]	113.8	90.7
			ΔH_{vap}	25.8[c]	24.4	25.8
			ρ_l	609[c]	610	620
	290	GEMC	P_{sat}	49.5[b]	49.2	46.3
			ΔH_{vap}	26.9[c]	25.4	26.7
			ρ_l	623[c]	629	634
	273.04	monophasic $P=0$	ΔH_{vap}	27.8[c]	26.5	27.5
			ρ_l	645[c]	656	647
	257.96	monophasic $P=0$	ΔH_{vap}	28.5[c]	27.2	28.0
			ρ_l	650[c]	670	659
	244.46	monophasic $P=0$	ΔH_{vap}	29.2[c]	27.6	28.9
			ρ_l	672[c]	681	676
	221.3	monophasic $P=0$	ΔH_{vap}	30.1[c]	28.9	30.0
			ρ_l	693[c]	707	698
	221.9	monophasic $P=0$	ΔH_{vap}	30.4[c]		30.4
			ρ_l	702[c]		706
	211.29	monophasic $P=0$	ΔH_{vap}	30.7[c]		30.6
			ρ_l	710[c]		709
n-octane	398.8	GEMC	P_{sat}	100[a]		86.5
			ΔH_{vap}	34.6[b]		34.7
			ρ_l	611[c]		617
	293	monophasic $P=0$	ΔH_{vap}	41.8[b]		41.2
			ρ_l	702[c]		706
n-dodecane	500	GEMC	P_{sat}	129[b]	209	
			ΔH_{vap}	43.4[b]	37.3	
			ρ_l	582[d]	540	
	458.34	GEMC	P_{sat}	45.0[b]	73.4	
			ΔH_{vap}	47.7[b]	42.6	
			ρ_l	630[c]	583	
	423.08	Monophasic NPT	ΔH_{vap}	50.9[b]	45.9	
			ρ_l	650[c]	629	
	392.87	Monophasic NPT	ΔH_{vap}	53.5[b]	48.1	
			ρ_l	674[c]	654	
	366.68	Monophasic NPT	ΔH_{vap}	55.6[b]	49.6	
			ρ_l	694[c]	671	
	343.76	Monophasic NPT	ΔH_{vap}	57.3[b]	51.8	
			ρ_l	712[c]	690	
	323.54	Monophasic NPT	ΔH_{vap}	58.8[b]	54.3	
			ρ_l	727[c]	715	
	289.49	Monophasic NPT	ΔH_{vap}	61.1[b]	57.3	
			ρ_l	752[c]	744	
n-eicosane	700	GEMC	P_{sat}	442[b]		422
			ΔH_{vap}	43.1[b]		40.3
			ρ_l	Ø		418
	633.58	GEMC	P_{sat}	140[b]		123
			ΔH_{vap}	55.1[b]		53.5
			ρ_l	Ø		507
	578.67	monophasic NPT	ΔH_{vap}	62.9[b]		60.0
			ρ_l	585[c]		563
	532.52	monophasic NPT	ΔH_{vap}	68.9[b]		65.3
			ρ_l	622[c]		600
	493.18	monophasic NPT	ΔH_{vap}	73.9[b]		70.6
			ρ_l	653[c]		641
	459.26	monophasic NPT	ΔH_{vap}	78.1[b]		73.1
			ρ_l	671[c]		657

[a]Reid *et al*. (Ref. 25).
[b]Correlations of the Dortmund Data Bank,[24] version 1998.
[c]Interpolated from Vargaftik (Ref. 23).
[d]Smith and Srivastava (Ref. 26).

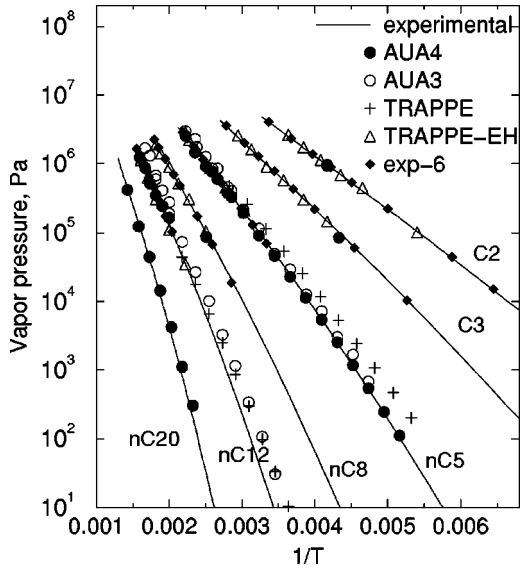

FIG. 1. Vapor pressures of *n*-alkanes computed with the new potential (AUA4), the potential of Toxvaerd (Ref. 7) (AUA3), the potential of Martin and Siepmann (Ref. 3, 5) (TRAPPE), the potential of Errington and Panagiotopoulos (Ref. 37) (exp-6), and the Hydrogen-explicit potential of Chen and Siepmann (Ref. 38) (TRAPPE-EH) compared with experimental data [correlations of the Dortmund data bank (Ref. 24), version 1998].

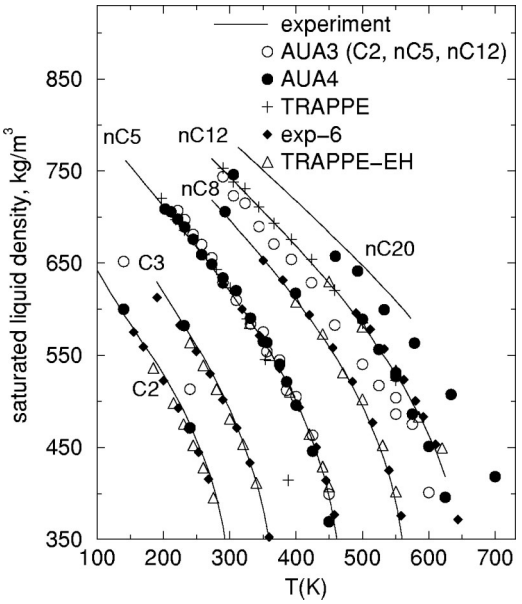

FIG. 3. Saturated liquid densities of *n*-alkanes computed with the new potential (AUA4), the potential of Toxvaerd (Ref. 7) (AUA3), the potential of Martin and Siepmann (Refs. 3, 5) (TRAPPE), the potential of Errington and Panagiotopoulos (Ref. 37) (exp-6), and the Hydrogen-explicit potential of Chen and Siepmann (Ref. 38) (TRAPPE-EH) compared with experimental data (Refs. 23, 24).

From Fig. 2, we can check that the behavior of the vaporization enthalpy satisfies the conditions required for thermodynamic integration. Indeed, the molar vaporization enthalpies of *n*-pentane, *n*-dodecane, and *n*-eicosane computed through Eq. (1) from NPT simulations at low temperatures are consistent with those computed by GEMC method at higher temperatures. Also, the derivative of the vaporization enthalpy vs. $1/T$ may be roughly approximated from two successive points while the second derivative estimated from three successive points would be erratic in sign. A numerical scheme of order three or above would therefore be useless, if not erroneous, since it requires implicitly that the second derivative is correct. This justifies the selection of a second-order integration scheme. Thanks to this method, we have extended the range of vapor pressure comparisons down to approximately 10 Pa, while previous investigations[3–5] did not consider vapor pressures lower than 20 kPa.

The comparison of equilibrium properties illustrated by Figs. 1, 2, and 3 shows that the AUA3 potential is a good potential for *n*-pentane, which was the major hydrocarbon investigated by Toxvaerd[7] while developing this potential. However AUA3 overestimates the liquid density for low molecular weight alkanes, such as ethane, and underestimates

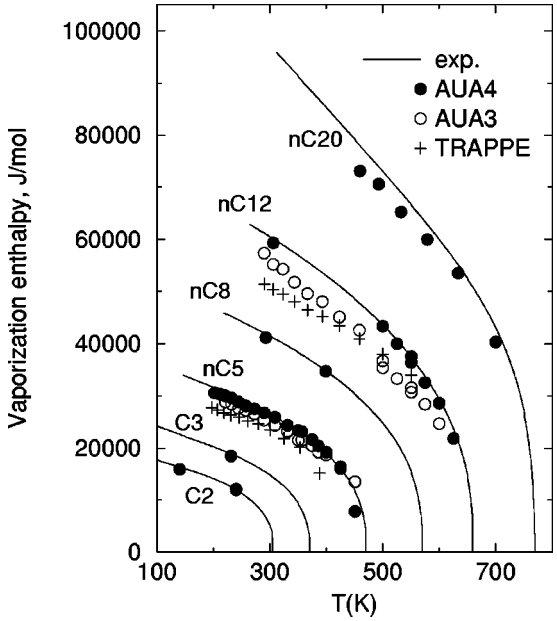

FIG. 2. Vaporization enthalpy of *n*-alkanes computed with the new potential (AUA4), the potential of Toxvaerd (Ref. 7) (AUA3), and the potential of Martin and Siepmann (Refs. 3, 5) (TRAPPE), compared with experimental data [correlations of the Dortmund data bank (Ref. 24), version 1998].

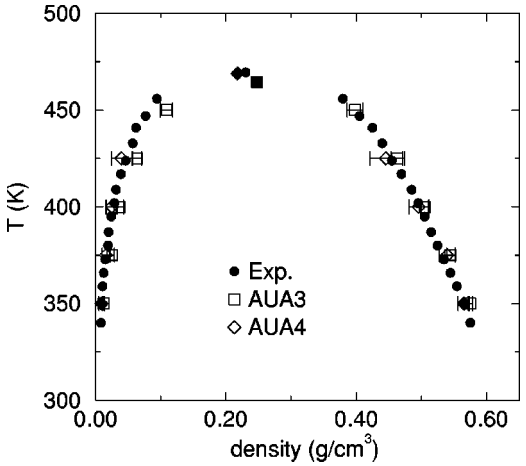

FIG. 4. Vapor–liquid coexistence density curve of *n*-pentane computed with the new potential (AUA4) and with the potential of Toxvaerd (Ref. 7) (AUA3), compared with experimental data (Ref. 26).

TABLE VI. Vapor pressures (P_{sat}, kPa), enthalpies of vaporization (ΔH_{vap}, kJ/mol), and coexisting densities (ρ_l, ρ_v, kg/m^3) of *n*-pentane, *n*-decane, and *n*-dodecane computed by GEMC with the new potential (AUA4) and with the AUA3 potential of Toxvaerd (Ref. 7). For *n*-pentane, the experimental coexisting densities have been taken from Smith and Srivastava (Ref. 26). The other experimental data are obtained through the correlations of the Dortmund Data Bank (Ref. 24) (version 1998).

Compound	T(K)	Property	Experimental data	AUA3	AUA4
n-pentane	350	P_{sat}	340	405	329
		ΔH_{vap}	23.2	21.5	23.3
		ρ_l	565	575	565
		ρ_v	9	12	9
	375	P_{sat}	578 (372 K)	855	601
		ΔH_{vap}	21.5 (372 K)	20.4	21.6
		ρ_l	538 (372 K)	545	540
		ρ_v	16 (372 K)	25	16
	400	P_{sat}	1080 (402 K)	1285	921
		ΔH_{vap}	18.76 (402 K)	18.6	19.2
		ρ_l	496 (402 K)	505	496
		ρ_v	30 (402 K)	37	29
	425	P_{sat}	1615 (424 K)	2294	1471
		ΔH_{vap}	16.17 (424 K)	16.0	16.3
		ρ_l	458 (424 K)	463	446
		ρ_v	48 (424 K)	64	40
	450	P_{sat}	2332 (446 K)	3008	2556
		ΔH_{vap}	12.52 (446 K)	13.5	7.8
		ρ_l	406 (446 K)	399	369
		ρ_v	78 (446 K)	109	102
n-decane	450	P_{sat}	109	205	115
		ΔH_{vap}	39.4	32.5	36.4
		ρ_l	599	572	603
		ρ_v	Ø	9	5
	475	P_{sat}	196	277	217
		ΔH_{vap}	36.9	30.4	34.8
		ρ_l	574	546	583
		ρ_v	10	13	8
	500	P_{sat}	330	578	335
		ΔH_{vap}	34.2	28.0	32.8
		ρ_l	531	511	552
		ρ_v	14	22	12
	525	P_{sat}	526	755	484
		ΔH_{vap}	31.1	25.1	29.9
		ρ_l	518	459	510
		ρ_v	Ø	31	19
	550	P_{sat}	800	1038	875
		ΔH_{vap}	27.5	22.2	27.9
		ρ_l	454	437	483
		ρ_v	48	58	35
n-dodecane	500	P_{sat}	129	278	165
		ΔH_{vap}	43.35	35.4	43.4
		ρ_l	582	537	589
		ρ_v	Ø	10	7
	525	P_{sat}	220	411	245
		ΔH_{vap}	40.43	33.3	40.03
		ρ_l	556	517	556
		ρ_v	Ø	19	11
	550	P_{sat}	355	682	358
		ΔH_{vap}	37.17	31.5	36.4
		ρ_l	529	504	527
		ρ_v	Ø	37	16
	575	P_{sat}	547	1318	520
		ΔH_{vap}	33.42	28.4	32.5
		ρ_l	498	475	486
		ρ_v	Ø	77	23
	600	P_{sat}	812	1701	878
		ΔH_{vap}	28.94	24.7	28.6
		ρ_l	463	401	451
		ρ_v	Ø	83	38
	625	P_{sat}	1168	Ø	1248
		ΔH_{vap}	23.1	Ø	21.8
		ρ_l	418	Ø	396
		ρ_v	Ø	Ø	65

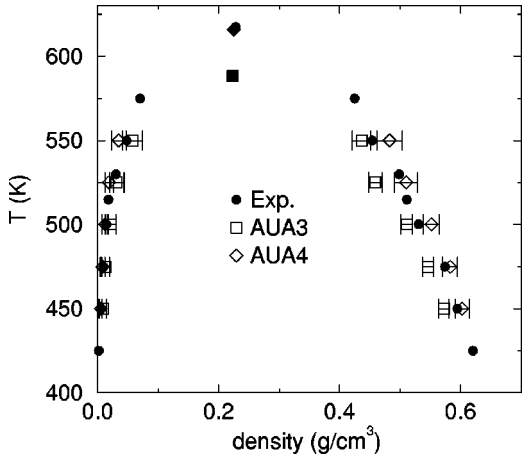

FIG. 5. Vapor–liquid coexistence density curve of *n*-decane computed with the new potential (AUA4) and with the potential of Toxvaerd (Ref. 7) (AUA3), compared with experimental data (Ref. 26).

it for heavier alkanes like *n*-dodecane. With the AUA4 potential, these deficiencies are corrected and most experimental data are closely reproduced. It is likely that the selection of identical Lennard-Jones diameters for CH_2 and CH_3 in the AUA3 potential is the main cause of the errors committed on liquid densities. Also, the AUA4 potential improves the description of vaporization enthalpies for heavy *n*-alkanes, which were underestimated by the AUA3 potential. The only systematic errors found significant with the AUA4 potential are related to the liquid densities and vaporization enthalpies of *n*-eicosane, particularly in the lower part of the temperature range investigated. Although rather long simulation runs were performed (1 to 1.5×10^6 stabilization steps and 2×10^6 production steps) it is possible that the system has not reached complete equilibrium and that high density configurations have not been sufficiently sampled. It must be stressed that the equilibration is very slow in the related simulations, which are performed at temperatures much lower than those where the Gibbs ensemble method is applicable.

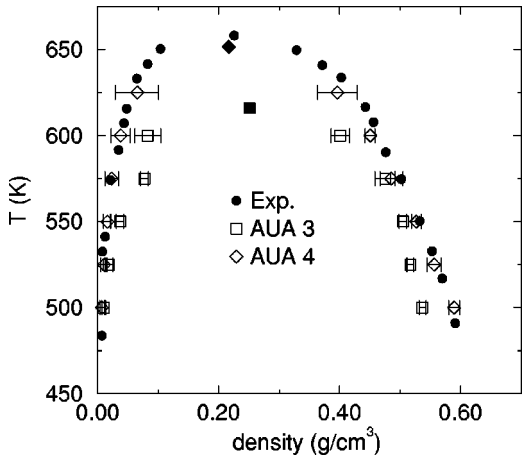

FIG. 6. Vapor–liquid coexistence density curve of *n*-dodecane computed with the new potential (AUA4) and with the potential of Toxvaerd (Ref. 7) (AUA3), compared with experimental data (Ref. 26).

TABLE VII. Critical parameters of *n*-alkanes computed from the new potential (AUA4) and from Toxvaerd's potential (Ref. 7) (AUA3) compared with two compilations of experimental data.

		Exp.[a]	Exp.[b]	AUA3	AUA4
n-pentane	T_c (K)	469.7	469.7	464.7	468.9
	ρ_c (kg/m^3)	230	237	247	218
n-decane	T_c (K)	617.5	617.7	588.3	615.7
	ρ_c (kg/m^3)	228	236	223	225
n-dodecane	T_c (K)	658.2	658.2	626.4	651.6
	ρ_c (kg/m^3)	226	239	252	217

[a]Reference 26.
[b]Reference 25.

The prediction of critical parameters from coexistence density curves (Table VII) shows a significant improvement of critical temperatures, which are now within 1% of experimental measurements. On the other hand, there is no clear evidence that critical densities are improved by AUA4. As illustrated by the significant differences between literature sources in Table VII, there is a large uncertainty on critical density measurements, especially for heavy hydrocarbons which are unstable at near-critical temperatures. Since the computed critical densities are also subject to significant uncertainties (estimated to be 5%%) we can only state that they appear compatible with experimental measurements. In order to make this point precise, a more thorough study involving larger box sizes and more reliable measurements would be needed.

It is highly satisfactory that the AUA4 potential, which has been optimized vs. pure component data only, provides also significant improvements vs. AUA3 when applied to CO_2–alkane mixtures. This is true for phase equilibrium properties and for volumetric properties as well. Although this good behavior should be confirmed by the investigation of other types of mixtures, it is an encouraging indication of the general applicability of the AUA4 potential for equilibrium properties. The use of the AUA4 potential together with the CO_2 potential of Harris and Yung seems to yield better predictions than calculations performed with the SKS united atoms potential by Cui *et al*.[34]

The investigation of transport properties, which is still preliminary, indicates that the AUA4 potential brings only slight improvements vs. the AUA3 potential. This is not surprising, since the investigated alkane, i.e., *n*-hexane, is already well reproduced by AUA3 because it is close to *n*-pentane. As a result, both potentials overestimate significantly the diffusion coefficient, particularly at low temperatures. It is possible that further progress in transport property prediction is possible by modifying the intramolecular potential, which has been unchanged in our study. Indeed, a recent study by Dysthe *et al*.[35] has pointed out that ''torsionally stiff molecules are less mobile than soft ones at high packing fractions,'' so that a consistent way of improving the model would be to narrow the width of the minima in the torsion potential.

An interesting question is whether the representation of equilibrium properties obtained with the optimized anisotropic united atoms potential could be obtained with an or-

TABLE VIII. Equilibrium properties of *n*-pentane and *n*-dodecane determined from the united atoms potential TRAPPE (Ref. 3) with the latest parameters set published by the authors (Ref. 5). Vapor pressures (P_{sat}) are given in kPa, vaporization enthalpies (ΔH_{vap}) in kJ/mol, liquid and vapor densities (ρ_l ,ρ_v) in kg/m^3.

Compound	T(K)	Property	Experimental data	TRAPPE
n-pentane	388.35	P_{sat}	820[a]	846
	GEMC	ΔH_{vap}	19.8[a]	15.2
		ρ_l	517[b]	414
		ρ_v	9 (at 350 K)[c]	21.0
	353.98	P_{sat}	375[a]	479
	GEMC	ΔH_{vap}	22.7	20.1
		ρ_l	562[b]	545
		ρ_v	9 (at 350 K)[c]	13.0
	325.2	P_{sat}	170[a]	263
	GEMC	ΔH_{vap}	24.8[a]	21.9
		ρ_l	594[b]	589
		ρ_v		7.5
	300.75	P_{sat}	75.2[a]	119
	GEMC	ΔH_{vap}	26.4[b]	23.4
		ρ_l	619[b]	625
		ρ_v	Ø	3.6
	279.72	P_{sat}	32.7[a]	53.7[d]
	Monophasic NPT	ΔH_{vap}	27.5[b]	24.7
		ρ_l	639[b]	643
	261.44	P_{sat}	13.9[a]	25.4[d]
	Monophasic NPT	ΔH_{vap}	28.3[b]	25.3
		ρ_l	653[b]	660
	245.4	P_{sat}	5.81[a]	11.8[d]
	Monophasic NPT	ΔH_{vap}	29.1[b]	25.9
		ρ_l	672[b]	675
	231.21	P_{sat}	2.37[a]	5.36[d]
	Monophasic NPT	ΔH_{vap}	29.6[b]	26.3
		ρ_l	684[b]	686
	218.58	P_{sat}	0.952[a]	2.41[d]
	Monophasic NPT	ΔH_{vap}	30.1[b]	26.8
		ρ_l	696[b]	697
	207.25	P_{sat}	0.372[a]	1.07[d]
	Monophasic NPT	ΔH_{vap}	30.5[b]	27.2
		ρ_l	705[b]	708
	197.04	P_{sat}	0.145[a]	0.468[d]
	Monophasic NPT	ΔH_{vap}	Ø	27.8
		ρ_l	714[b]	720
n-dodecane	550	P_{sat}	355[a]	368
	GEMC	ΔH_{vap}	37.2[a]	33.9
		ρ_l	529[c]	523
		ρ_v	Ø	15
	500	P_{sat}	129[a]	155
	GEMC	ΔH_{vap}	43.4[a]	38.0
		ρ_l	582[c]	585
		ρ_v	Ø	6.7
	458.34	P_{sat}	45.0[a]	44.3
	GEMC	ΔH_{vap}	47.7[a]	41.0
		ρ_l	630[b]	621
		ρ_v	Ø	2.0
	423.08	P_{sat}	15.2[a]	17.9[d]
	Monophasic NPT	ΔH_{vap}	50.9[a]	43.4
		ρ_l	650[b]	654
	392.87	P_{sat}	4.89[a]	6.63[d]
	Monophasic NPT	ΔH_{vap}	53.5[a]	45.2
		ρ_l	674[b]	676
	366.68	P_{sat}	1.49[a]	2.48[d]
	Monophasic NPT	ΔH_{vap}	55.6[a]	46.5
		ρ_l	694[b]	693
	343.76	P_{sat}	0.433[a]	0.869[d]
	Monophasic NPT	ΔH_{vap}	57.3[a]	48.1
		ρ_l	712[b]	711
	323.54	P_{sat}	0.121[a]	0.303[d]
	Monophasic NPT	ΔH_{vap}	58.8[a]	49.5
		ρ_l	727[b]	731
	305.57	P_{sat}	0.0324[a]	0.100[d]
	Monophasic NPT	ΔH_{vap}	60.0[a]	50.3
		ρ_l	740[b]	738
	289.49	P_{sat}	0.00842[a]	0.0336[d]
	Monophasic NPT	ΔH_{vap}	61.1[a]	51.5
		ρ_l	752[b]	753

[a]Correlations of the Dortmund data bank (Ref. 24), version 1998.
[b]Interpolated from Vargaftik (Ref. 23).
[c]Smith and Srivastava (Ref. 26).
[d]Thermodynamic integration.

TABLE IX. Simulation results on the binary mixtures carbon dioxide–alkane mixtures. The AUA3 results are taken from Delhommelle *et al*. (Ref. 30). The experimental data are taken from Besserer and Robinson (Ref. 28) for the carbon dioxide–*n*-pentane mixture, and from Reamer and Sage (Ref. 29) for the carbon dioxide–*n*-decane mixture.

Binary Mixture	P (bar)	Property	Experimental data	AUA3	AUA4
Carbon Dioxide –*n*-pentane	22.421	X CO2	0.163	0.179	Ø
		Y CO2	0.843	0.796	Ø
		ρ_l	581	590	Ø
$T=344.16$ K		ρ_v	45	44	Ø
	30.055	X CO2	0.225	0.238	0.288
		Y CO2	0.873	0.856	0.889
		ρ_l	584	593	596
		ρ_v	62	59	57
	39.271	X CO2	0.303	0.356	0.352
		Y CO2	0.894	0.880	0.896
		ρ_l	587	599	607
		ρ_v	83	79	77
	49.519	X CO2	0.39	0.440	0.446
		Y CO2	0.904	0.893	0.915
		ρ_l	592	603	611
		ρ_v	109	104	100
	58.735	X CO2	0.47	0.505	0.540
		Y CO2	0.911	0.903	0.930
		ρ_l	593	609	612
		ρ_v	137	128	124
	68.982	X CO2	0.562	0.566	Ø
		Y CO2	0.913	0.906	Ø
		ρ_l	590	611	Ø
		ρ_v	175	160	Ø
Carbon Dioxide –*n*-decane	13.79	X CO2	0.058	0.071	0.075
		Y CO2	0.823	0.721	0.834
		ρ_l	573	538	572
$T=477$ K		ρ_v	Ø	27	22
	41.37	X CO2	0.186	0.238	0.203
		Y CO2	0.926	0.883	0.905
		ρ_l	571	531	582
		ρ_v	Ø	63	60
	55.16	X CO2	0.245	0.322	0.269
		Y CO2	0.935	0.901	0.920
		ρ_l	569	522	581
		ρ_v	Ø	83	78
	68.95	X CO2	0.299	0.385	0.356
		Y CO2	0.938	0.915	0.945
		ρ_l	566	520	564
		ρ_v	98	103	94

dinary united atoms potential, i.e., with the force center on carbon atoms. The tests performed with the TRAPPE potential of Martin and Siepmann[3,5] (Table VIII) indicate that this

TABLE X. Self-diffusion coefficients computed by molecular dynamics simulations for liquid *n*-hexane at atmospheric pressure.

T (K)	Density[a] (kg/m^3)	Self-diffusion coefficient (10^{-9} m^2/s) Exp.[a]	AUA3	AUA4
223.15	719	1.32	1.9	1.9
273.15	677	2.96	3.8	3.6
333.15	622	5.97	6.6	6.3

[a]Reference 31.

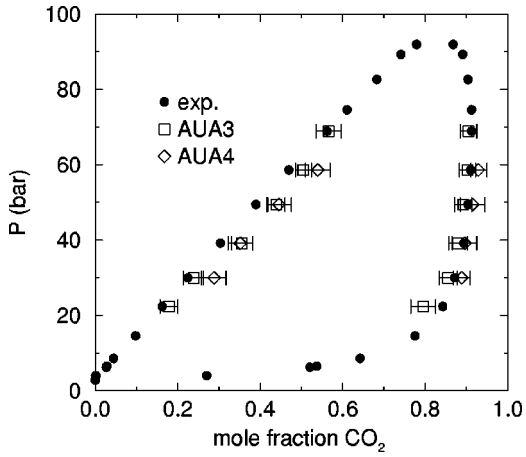

FIG. 7. Phase diagram of the CO_2–*n*-pentane mixture at 344.16 K. The AUA3 results are taken from Delhommelle (Ref. 30) and the experimental data from Besserer and Robinson (Ref. 28).

potential represents very well the liquid densities and reasonably well the vapor pressures of *n*-pentane and *n*-dodecane in the region of high reduced temperatures ($T/T_c>0.6$), i.e., the region where GEMC is feasible. However, the significant underestimation of vaporization enthalpies causes the vapor pressures to depart increasingly from experimental values at low temperatures, as it plays a major role in the integration of the Clapeyron Eq. (2). In their development of the SKS and NERD united atoms potentials, the authors[2,4] investigated reduced temperatures larger than 0.6 and gave no comparison with vaporization enthalpies, so that the applicability of these models to lower temperatures is unclear. It cannot be excluded that the united atoms potential has an insufficient number of degrees of freedom to allow for a simultaneous representation of liquid densities, vapor pressures, and vaporization enthalpies in a large range of carbon numbers and temperatures. If transport properties are considered, the anisotropic united atoms provide generally better predictions than united atoms potentials in dense phases.[36] As both types of potentials require equivalent computing time, the aniso-

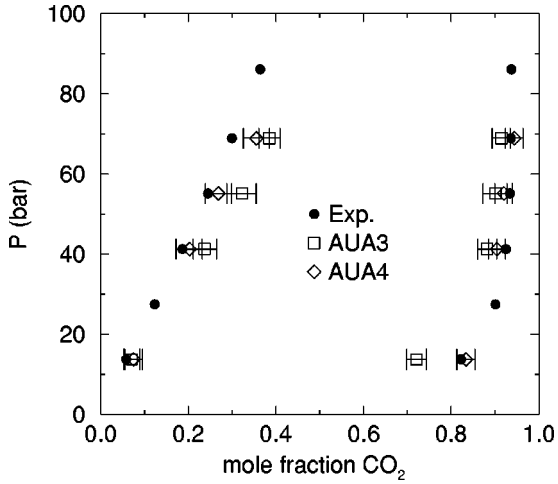

FIG. 8. Phase diagram of the CO_2–*n*-decane mixture at 477 K. The AUA3 results are taken from Delhommelle (Ref. 30) and the experimental data from Reamer and Sage (Ref. 29).

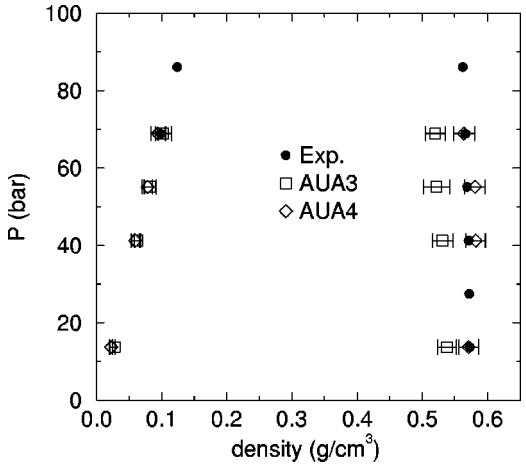

FIG. 9. Equilibrium densities of the CO_2–*n*-decane system at 477 K [experimental data from Reamer and Sage (Ref. 29)].

tropic united atoms appears therefore superior to ordinary united atoms potentials for further development and exploitation. When comparison is extended to the most recent potentials of *n*-alkanes,[37,38] AUA4 performs similarly well on average (Figs. 1 and 3). It is likely that these potentials are more accurate than AUA4 in the usual temperature range investigated in molecular simulation of phase equilibria (i.e., reduced temperatures above 0.6). However, our model has been developed and tested in a larger temperature range, comprising much lower temperatures. For heavy hydrocarbons, this is an important point because numerous industrial applications imply moderate or low temperatures. Also, we may point out that the potential of Errington and Panagiotopoulos[37] requires three parameters per interaction site, so that three mixing rules are needed instead of two in the anisotropic united atoms potential. The selection of the mixing rules on the repulsion parameters will be more delicate in future extensions of this potential to other functional groups than with the AUA potentials. The potential of Chen and Siepmann[38] considers explicit hydrogens, i.e., three to four times more interaction sites per molecule than our potential. As a result, it will be always limited to treat systems

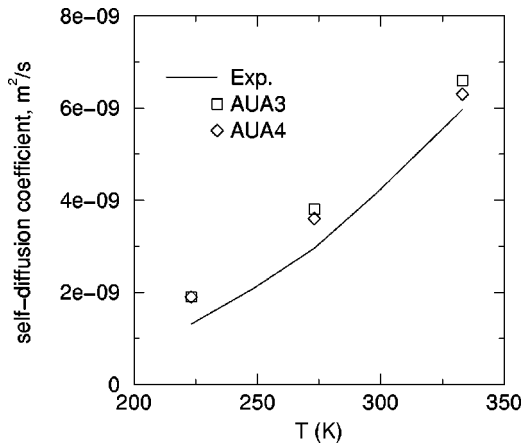

FIG. 10. Self-diffusion coefficients computed by molecular dynamics simulations for liquid *n*-hexane at atmospheric pressure [experimental data from Harris (Ref. 31)].

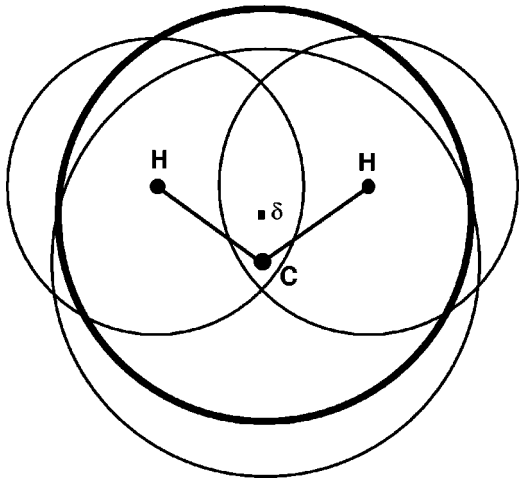

FIG. 11. Exclusion sphere of the CH_2 group in the AUA4 potential (heavy line) compared with the exclusion spheres of the constituting carbon and hydrogen groups (thin lines). δ is the force center of the group. The view is taken perpendicular to the plane containing the carbon and the hydrogen atoms of the group.

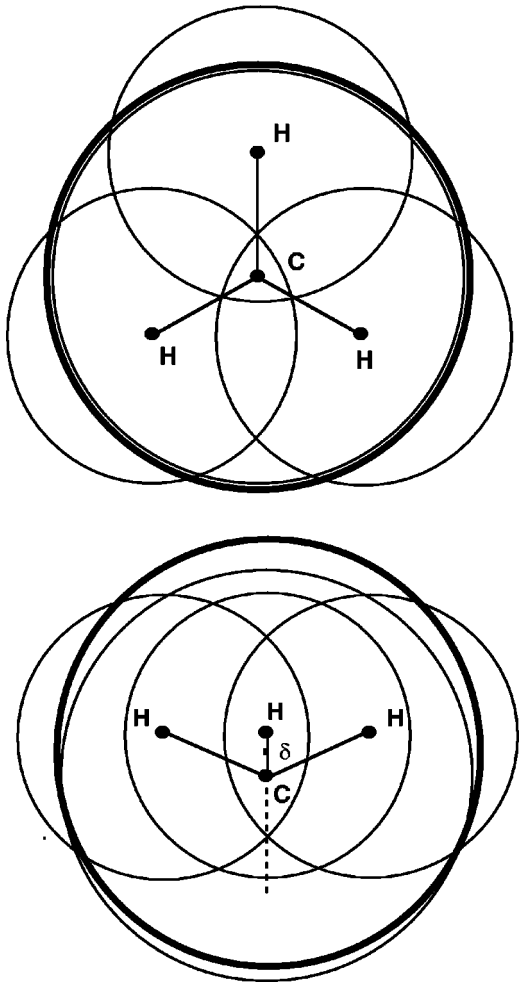

FIG. 12. Exclusion sphere of the CH_3 group in the AUA4 potential (heavy line) compared with the exclusion spheres of the constituting carbon and hydrogen groups (thin lines). δ is the force center of the group. *Top*: view taken perpendicular to the plane containing the three hydrogen atoms of the group. *Bottom*: view taken perpendicular to the ternary symmetry axis of the group, parallel to one of its binary symmetry planes.

three or four times smaller than our potential for a given computer time. Such detail in the molecular representation of alkanes appears unnecessary to match the properties considered in our study.

VI. CONCLUSIONS

The present study has shown that it is possible to optimize further the parameters of the anisotropic united atoms potential, AUA3, proposed by Toxvaerd[7] for *n*-alkanes, using several equilibrium properties (vapor pressures, vaporization enthalpies, and liquid densities) of selected compounds as reference experimental data. The optimized Lennard-Jones parameters of the CH_2 and CH_3 groups form regular sequences with those of methane, which show that they have a good physical sense. Similarly, the shift of the force centers from the carbon atoms still places them at reasonable positions between the carbon and hydrogen atoms of the groups. As the carbon–carbon distances and average bond angles have been fixed identical for all chain lengths, the optimized potential is applicable to any *n*-alkane without experimental information, which was not the case for the AUA3 potential.

The optimized potential, called AUA4, has been shown to predict the equilibrium properties of pure *n*-alkanes in a large range of temperature and carbon number. For instance, the use of thermodynamic integration has allowed to test successfully the AUA4 potential against a large range of vapor pressures (100 Pa to 2 MPa), that extends several orders of magnitude below previous investigations toward low temperatures. The new potential has been also successfully applied to the prediction of phase equilibria and volumetric properties of CO_2–alkane mixtures. As it involves only a very minor computational overhead compared to united atoms potentials, it is a privileged model for the prediction of equilibrium properties.

Concerning transport properties, the AUA4 potential shows slightly improved predictions compared to the AUA3 potential from the few simulations performed on *n*-hexane. Both models overestimate self-diffusion coefficients, particularly at low temperature.

Among the perspectives opened by this work, the optimization of the intramolecular parameters for *n*-alkanes (particularly those characterizing the torsion potential) would probably improve transport property prediction in dense liquids, while maintaining a satisfactory representation of thermodynamic properties. This would result in a transferable model particularly useful for industrial applications. Another favorable perspective is the extension of the anisotropic united atoms potential to other families like isoalkanes, cycloalkanes, olefins, etc. in the same way as achieved with UA potentials.[5,36] It is indeed likely that improvements similar to *n*-alkanes can be obtained with these compounds.

ACKNOWLEDGMENTS

The authors thank B. Neubauer and D. Dysthe for interesting discussions and advice about this work, and A. Z. Panagiotopoulos for access to data files of simulation results. J.D. thanks the Institut Français du Pétrole for financial support through a BDI CNRS/IFP grant.

[1] W. L. Jorgensen, J. D. Madura, and C. J. Swenson, J. Am. Chem. Soc. **106**, 813 (1984).
[2] B. Smit, S. Karaborni, and J. I. Siepmann, J. Chem. Phys. **102**, 2126 (1995).
[3] M. G. Martin and J. I. Siepmann, J. Phys. Chem. B **102**, 2569 (1998).
[4] S. A. Nath, F. A. Escobedo, and J. J. de Pablo, J. Chem. Phys. **108**, 9905 (1998).
[5] M. G. Martin and J. I. Siepmann, J. Phys. Chem. B **103**, 4508 (1999).
[6] S. Toxvaerd, J. Chem. Phys. **93**, 4290 (1990).
[7] S. Toxvaerd, J. Chem. Phys. **107**, 5197 (1997).
[8] P. Padilla and S. Toxvaerd, J. Chem. Phys. **94**, 5650 (1991).
[9] J. Delhommelle, A. Boutin, B. Tavitian, A. Mackie, and A. H. Fuchs, Mol. Phys. **96**, 1517 (1999).
[10] D. Dysthe, A. H. Fuchs, and B. Rousseau, J. Chem. Phys. **110**, 4047 (1999).
[11] D. Dysthe, A. H. Fuchs, and B. Rousseau, J. Chem. Phys. **110**, 4060 (1999).
[12] A. Panagiotopoulos, Mol. Phys. **61**, 813 (1987).
[13] B. Smit, S. Karaborni, and J. I. Siepmann, J. Phys. Chem. **102**, 2126 (1995).
[14] K. Esselink, L. D. J. C. Loyens, and B. Smit, Phys. Rev. E **51**, 1560 (1995).
[15] A. D. Mackie, B. Tavitian, A. Boutin, and A. H. Fuchs, Mol. Simul. **19**, 1 (1997).
[16] M. P. Allen and D. J. Tildesley, *Computer Simulation of Liquids* (Oxford Science, Oxford, 1987).
[17] D. A. Kofke, J. Chem. Phys. **98**, 4149 (1993).
[18] J. M. Simon, D. K. Dysthe, A. H. Fuchs, and B. Rousseau, Fluid Phase Equilibria **150-151**, 150 (1998).
[19] *Handbook of Chemistry and Physics*, 73rd ed. edited by D. R. Lide (CRC, New York, 1992).
[20] R. L. Hilderbrandt, J. D. Wieser, and L. K. Montgomery, J. Am. Chem. Soc. **95**, 8598 (1973).
[21] K. Palmö, N. G. Mirkin, L. O. Pietila, and S. Krimm, Macromolecules **26**, 6831 (1993).
[22] S. Fitzwater and L. S. Bartell, J. Am. Chem. Soc. **98**, 5107 (1976).
[23] N. B. Vargaftik, *Tables on the Thermophysical Properties of Liquids and Gases*, 2nd ed. (Wiley, New York, 1975).
[24] J. Gmehling, CODATA Bulletin **58**, 56 (1985).
[25] R. C. Reid, J. M. Prausnitz, and B. E. Poling, *The Properties of Gases and Liquids*. 4th ed. (McGraw-Hill, New York, 1986), p. 741.
[26] B. D. Smith and R. Srivastava, *Thermodynamics of Pure Compounds: Hydrocarbons and Ketones* (Elsevier, New York, 1986).
[27] J. G. Harris and K. H. Yung, J. Phys. Chem. **99**, 12021 (1995).
[28] G. J. Besserer and D. B. Robinson, J. Chem. Eng. Data **18**, 416 (1973).
[29] H. H. Reamer and B. H. Sage, J. Chem. Eng. Data **8**, 509 (1963).
[30] J. Delhommelle, A. Boutin, and A. H. Fuchs, Mol. Simul. **22**, 351 (1999).
[31] K. R. Harris, J. Chem. Soc., Faraday Trans. 1 **78**, 2265 (1982).
[32] D. Möller, J. Oprzynski, A. Müller, and J. Fischer, Mol. Phys. **75**, 363 (1992).
[33] W. L. Jorgensen, D. S. Maxwell, and J. Tirado-Rives, J. Am. Chem. Soc. **118**, 11225 (1996).
[34] S. T. Cui, H. D. Cochran, and P. T. Cummings, J. Phys. Chem. B **103**, 4485 (1999).
[35] D. K. Dysthe, A. H. Fuchs, and B. Rousseau, J. Chem. Phys. (submitted).
[36] B. Neubauer, A. Boutin, B. Tavitian, and A. H. Fuchs, Mol. Phys. **97**, 769 (1999).
[37] J. R. Errington and A. Z. Panagiotopoulos, J. Phys. Chem. B **103**, 6314 (1999).
[38] B. Chen and J. I. Siepmann, J. Phys. Chem. B **103**, 5370 (1999).